Journal of Zhejiang University-SCIENCE B (Biomedicine & Biotechnology) *in press*
www.jzus.zju.edu.cn; www.springer.com/journal/11585
E-mail: jzus_b@zju.edu.cn

Research Article
https://doi.org/10.1631/jzus.B2300678

Role of PANoptosis and related genes in acute liver failure: neoteric insight from bioinformatic analysis and animal experiment verification

Tiantian GE[1]*, Yao CHEN[1]*, Lantian PANG[2], Junwei SHAO[3]✉, Zhi CHEN[1]✉

[1]*State Key Laboratory for Diagnosis and Treatment of Infectious Diseases, National Clinical Research Center for Infectious Diseases, National Medical Center for Infectious Diseases, Collaborative Innovation Center for Diagnosis and Treatment of Infectious Diseases, The First Affiliated Hospital, Zhejiang University School of Medicine*
[2]*The Department of Infectious Diseases, The Second Affiliated Hospital, Zhejiang University School of Medicine, 88 Jiefang Road, Hangzhou, 310003, Zhejiang, China*
[3]*Division of Hepatobiliary and Pancreatic Surgery, Department of Surgery, The Second Affiliated Hospital, School of Medicine, Zhejiang University, 88 Jiefang Road, Hangzhou, 310009, China*

Abstract
Background: PANoptosis has the features of pyroptosis, apoptosis and necroptosis. Numerous studies have confirmed the diverse roles of various types of cell death in acute liver failure (ALF), but limited attention has been given to the crosstalk among them. In this study, we aimed to explore the role of PANoptosis in ALF and uncover new targets for its prevention or treatment.
Methods: Three ALF-related datasets (GSE14668, GSE62029, GSE74000) were downloaded from the Gene Expression Omnibus (GEO) database to identify differentially expressed genes (DEGs). Hub genes were identified through intersecting DEGs, genes obtained from weighted gene co-expression network analysis (WGCNA) and genes related to PANoptosis. Gene ontology (GO), Kyoto Encyclopedia of Genes and Genomes (KEGG), protein-protein interaction (PPI) analyses and gene set enrichment analysis (GSEA) were performed to determine functional roles. Verification was performed using an ALF mouse model.
Results: Our results showed that expression of seven hub genes (BMF, BNIP3L, CASP1, RIPK3, UACA, UNC5B, ZBP1) was up-regulated in liver samples of patients. However, in the ALF mouse model, the expression of BNIP3L, RIPK3, P-RIPK3, UACA and cleaved caspase1 was up-regulated, while expression of CASP1 and UNC5B was down-regulated. The expression of ZBP-1 and BMF increased only during the development of ALF, and there was no significant change in the end stage. Immunofluorescence of mouse liver tissue showed that macrophages expressed all seven markers. Western blot results showed that pyroptosis, apoptosis and necroptosis were always involved in LPS/D-gal induced ALF mice. The ALF cell model showed that bone marrow derived macrophages (BMDMs) form PANoptosomes after LPS stimulation.
Conclusion: Our results suggest that PANoptosis of macrophages promotes the development of ALF. Seven new ALF biomarkers identified and validated in this study may contribute to further investigation of diagnostic markers or novel therapeutic targets of ALF.

Keywords: Acute liver failure, PANoptosis, GEO, Biomarkers, Therapeutic target

✉ Zhi CHEN, zjuchenzhi@zju.edu.cn
Junwei SHAO, sjw507@163.com
* The two authors contributed equally to this work
Tiantian GE, https://orcid.org/0000-0002-6595-6949
Yao CHEN, https://orcid.org/0009-0002-4717-3147
Zhi CHEN, https://orcid.org/0000-0002-0848-1502
Junwei SHAO, https://orcid.org/0000-0002-7418-0230

Received Sept. 19, 2023; Revision accepted Apr. 23, 2024;
Crosschecked xxx xx, xxxx; Published online xxx xx, xxxx

© Zhejiang University Press 2024

unedited

1. Introduction

Acute liver failure (ALF) is a lethal liver disease that can occur after exposure to virus, alcohol, drugs or an autoimmune response, and is characterized by coagulopathy, encephalopathy and hepatic metabolic dysfunction (Bernal and Wendon, 2013; Stravitz and Lee, 2019). The first period of ALF involves direct interaction between stimuli and hepatocytes, and the secondary host inflammatory response after cell death results in organ failure (Khan et al., 2006). Currently, liver transplantation is the only definitive treatment for ALF, indicating that our current understanding of its mechanism is insufficient.

According to the Nomenclature Committee on Cell Death (NCCD), there are two categories of cell death: accidental cell death (ACD) and regulated cell death (RCD) (Galluzzi et al., 2015). ACD is induced by severe insults which are not considered as a target for therapeutic intervention because they cannot be modulated or prevented (Green and Kroemer, 2005; Long and Ryan, 2012). In contrast, RCD can be interrupted by means of genetic or pharmacologic interventions targeted to the key components because its process involves molecular regulatory mechanisms such as apoptosis, necroptosis, pyroptosis and ferroptosis, coded by genes (Galluzzi et al., 2014; Galluzzi, et al., 2015). Although many studies have identified their respective roles in ALF (Schwabe and Luedde, 2018; Wang et al., 2021; Zheng et al., 2022), a growing body of studies has shown extensive molecular crosstalk among these mechanisms rather than being independent of each other, as previously suggested (Kuriakose et al., 2016; Malireddi et al., 2018). Therefore, it is very important to explore the mechanisms involved in the different RCD pathways.

PANoptosis is a new concept proposed by Malireddi in 2019 that has the characteristics of apoptosis, pyroptosis and necroptosis, but cannot be represented solely by any one of them. PANoptosis is triggered by the PANoptosome, a multimeric protein complex that integrates the components from other RCD pathways (Malireddi et al., 2019; Christgen et al., 2020). Although initial studies related to PANoptosis involved diseases caused by bacterial or viral infections, subsequent studies have shown that PANoptosis is also present in some tumor and ischemic-related diseases (Karki et al., 2021b; Lin et al., 2022; Nguyen and Kanneganti, 2022; Yan et al., 2023). ALF is caused by cytokine storms generated by an excessive immune response and one of its clinical manifestations is coagulation dysfunction. Both of these features may provide evidence for a possible relationship between PANoptosis and ALF. In this study, we used bioinformatics methods and an animal ALF model to identify the hub genes of PANoptosis in ALF. These results provide important directions for further study of the diagnosis, progression, and targeted therapy of ALF.

unedited

2. Methods

2.1 Microarray Data

Three sets of ALF-related transcriptome datasets, GSE14668, GSE62029, GSE74000, were downloaded from the Gene Expression Omnibus (GEO) database (www.ncbi.nlm.nih.gov/geo/). Fig. 1 depicts the study flowchart.

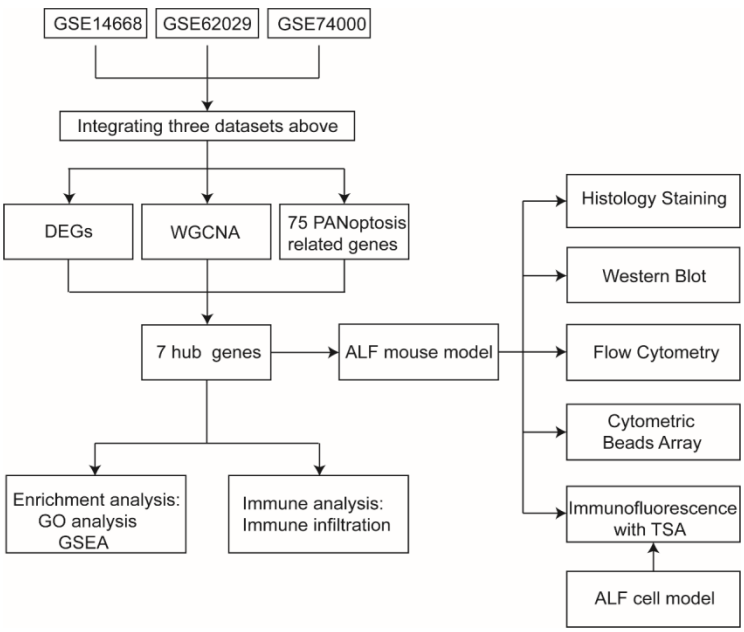

Fig. 1 Flow diagram of the study process

2.2 Grouping setting

We used the transcriptome data of liver donors as a control group, and the transcriptome data of patients with HBV-associated or APAP-induced ALF as the ALF group. Transcriptome data from normal liver tissue of patients with angioma were excluded due to concerns that angioma might impact the results. We treated specimens from the same patient as independent samples that did not require exclusion or merging, as our study did not involve the patients' clinical information, and the gene expression profiles of these specimens were distinct.

2.3 Data processing and identification of differentially expressed genes (DEGs)

Normalization, log2 transformation and merging of the three ALF raw datasets were performed using the "inSilicoMerging" package in R software. The Bioconductor "SVA" package was applied to the combined dataset to eliminate batch effects (Leek et al., 2012). The Limma package was used to screen the DEGs, with the criterion set as |log2 fold change (FC)| >1.5 and an adjusted P value of <0.05.

2.4 Weighted gene co-expression network analysis (WGCNA)

Initially, we calculated the median absolute deviation (MAD) for each gene based on gene expression profiles. Subsequently, the lower 50% of genes with the smallest MAD values were removed. Next, we used the goodSamplesGenes function from the WGCNA package in R software to eliminate outliers from both genes and samples. Additionally, we developed a scale-free co-expression network and identified a β shrinkage parameter value of β=24 following the scale-free topology criterion. Lastly, genes exhibiting similar expression patterns were grouped into modules using the "dynamic tree-cutting" algorithm, and the correlation between sample traits and module genes was assessed through Pearson's correlation analysis.

2.5 Identification of Hub genes

The "VennDiagram" package in R software was used to obtain hub genes associated with PANoptosis and ALF by intersecting DEGs, genes obtained from WCGNA and genes related to PANoptosis. The differences in expression of hub genes between ALF and healthy samples were represented by violin plots. The T-test was used for the data that conformed to a normal distribution while the Mann-Whitney U-test was used for data with a non-normal distribution. Significance was defined as P <0.01.

2.6 Functional Enrichment Analysis

Gene Ontology (GO) and Kyoto Encyclopedia of Genes and Genomes (KEGG) analyses were carried out to compare the differential signal pathway and biological effects among the 7 genes. We used the Metascape database for annotation and the Sangerbox for visualization. We set the

unedited

min overlap to 1, since the number of hub genes selected was too small, and the *P* value cutoff was set to <0.05.

2.7 Potential interaction between hub genes

First, we used the STRING database to obtain the interaction relationships among the 7 hub genes, and then we gradually expanded the interaction relationship between hub genes until 7 genes were connected in a network. Cytoscape was then used to remove the non-hub genes whose total number of adjacent hub genes was less than 3. The final result was a predicted interaction between hub genes.

2.8 Gene set enrichment analysis

We performed gene set enrichment analysis (GSEA) using GSEA software (version 4.0.3). According to the expression level of target genes, the samples were divided into high-expression groups (>=50%) and low-expression groups (<=50%). The relevant pathways and molecular mechanisms were evaluated based on gene expression profiles and phenotypic grouping by the Molecular Signatures Database. We set the minimum gene set to 5 and the maximum gene set to 5000. A *P* value of <0.05 and FDR of <0.25 were considered statistically significant.

2.9 Analysis of immune infiltration

The abundance of 22 subtypes of immune cells was determined after analyzing the sequencing data of ALF samples using the CIBERSORT algorithm. These subtypes represent the cellular composition of the immune microenvironment in ALF, and Spearman correlation analysis was performed on genes and immune cells.

2.10 Mouse model of ALF

An ALF mouse model was established in randomly assigned eight-week-old C57BL/6 mice (Gampharmatech, Shanghai, China) by intraperitoneal injection (i.p) of LPS (40 μg/kg, Sigma, L4391) and D-galactosamine (800 mg/kg, Sigma, G0500) (LPS/D-gal) (Li et al., 2021) after overnight starvation. Control group mice received the same volume of PBS. To evaluate the extent of liver injury, liver tissues and serum samples were collected at 0.5, 1, 2, 4 and 6 h after LPS/D-gal injection while samples of the control group were collected at 6 h after PBS injection. Serum levels of ALT and AST were measured using a standard analyzer, DRI-CHEM 4000ie (FUJIFILM). Cytokine levels in the serum were assessed using the BD Cytometric Bead Array Mouse Inflammation Kit (BD Biosciences) and analyzed by flow cytometry.

2.11 Hematoxylin and eosin staining

Liver tissues were fixed in 4% paraformaldehyde (PFA) and then embedded in paraffin. Sections with a thickness of 5 μm were prepared and subjected to staining with hematoxylin and eosin (H&E).

2.12 Western blot

The liver tissue was cleaved into RIPA containing protease inhibitor and phosphatase inhibitor by a tissue grinder, and incubated on ice for 30 min with vortex oscillation once every 10 min, and then centrifuged at 12000g for 15 min at 4 °C. After being quantitatively measured by BCA solution, the tissue homogenate was boiled in a metal bath at 100 °C for 10 min after being mixed with 5X loading buffer. The mixture was used for western blotting. The antibodies used included BMF (CST, 50542s), BNIP3L (CST, 12396T), Caspase1 (Proteintech, 81482-1-RR), Cleaved caspase1 (CST, 89332s), Cleaved caspase3 (CST, 9664), Cleaved caspase8 (CST, 8592), GAPDH (Proteintech, 60004-1-Ig) , GSDMD (Huabio,er1907-37), GSDME (Proteintech,13075-1-AP), Goat Anti-Mouse IgG (Proteintech, SA00001-1), Goat Anti-Rabbit IgG (Proteintech, SA00001-2), MLKL (CST, 98110), P-MLKL (CST, 98110), P-RIPK3 (CST, 98110), RIPK3 (CST, 98110), UACA (Absin, abs119046), UNC5B (CST, 13851s), and ZBP1 (Invitrogen, PA5-20455).

2.13 Isolation of liver immune cells

In brief, liver tissue was shredded by tweezers in digestive fluid containing type IV collagenase and DNase, and then transferred to a constant temperature shaker at 37 °C for further digestion. Next, the liver tissue suspension was filtered with a 70-um filter. The filtrate was used to precipitate liver cells at a centrifugation rate of 50g, and the supernatant containing immune cells was precipitated at a rate of 500g. Finally, the immune cells were precipitated by centrifugation in

unedited

33.3% Percoll working solution. The immune cells were washed with PBS for subsequent flow cytometry analysis.

2.14 Flow cytometry

A BD LSRFortessa cell analyzer was used for flow cytometry. The following fluorescent antibodies were used: anti-CD45-FITC (Biolegend, 103108), anti-CD11b-APC (Biolegend, 101212), anti-F4/80-BV421 (Biolegend, 123131), and anti-7AAD-APC/Cy7 (Biolegend, 420404).

2.15 Immunofluorescence with tyramide signal amplification (TSA)

Paraffin sections were dewaxed and treated for antigen retrieval, and the endogenous peroxidase was removed with 3% hydrogen peroxide. Next, each antigen was stained with primary and secondary antibodies and signal was amplified with fluorescent staining of different channels according to the instructions. Finally, the nuclei were labeled with DAPI. Antibodies used for immunofluorescence included ani-BMF (Qcheng bio,QC330Hu01), anti-BNIP3L (Proteintech, 68118-1-Ig), anti-CASP1 (Proteintech, 81482-1-RR), anti-RIPK3 (Proteintech, 17563-1-AP), anti-UACA (Proteintech, 25654-1-AP), anti-UNC5B (Huabio, ER1918-41), anti ZBP1(Invitrogen, PA5-143928), anti-F4/80 (Proteintech, 29414-1-AP), anti-CD11b (Servicebio, GB115689), anti-ly6c(Servicebio, GB115601), and anti-CASP8 (Proteintech, 66093-1-Ig).

2.16 Verification the formation of PANoptosome on ALF cell model

Bone marrow cells were extracted from the femur and tibia of mice and cultured in DMEM medium (DMEM supplemented with 10% heat-inactivated FBS, 100 U/mL penicillin, 100 μg/mL streptomycin, and 50 ng/mL M-CSF). The cells were cultured for three days and then provided with fresh DMEM medium. Mature BMDMs were harvested after seven days of culture and seeded in 12-well glass-bottom plates at a concentration of 2*105 cells/mL in complete DMEM medium containing 100-mM glutamine. The cells were incubated at 37 °C in a humidified atmosphere with 5% CO2 overnight for experiments. The following day, the BMDMs were stimulated with LPS (100 ng/mL) for 6 h, followed by immunofluorescence staining using TSA for cell imaging.

2.17 Statistical analysis

All data are presented as mean ± standard deviation. The Shapiro-Wilk normality test was conducted to assess the normality of the distribution of the data. For comparisons between two groups, an independent samples t-test was used. In cases where a normal distribution was not observed, the Mann-Whitney U test was used. In the presence of a normal distribution, one-way ANOVA was used to compare three or more groups, followed by Tukey's multiple comparison tests for post-hoc analysis. In instances where a normal distribution was not present, the Kruskal-Wallis test was performed and then a Dunn multiple comparison test was applied for post-hoc analysis. Spearman's rank test was used to evaluate correlations: -, P >0.05; *, P <0.05; **, P <0.01; ***, P <0.001; ****, P <0.0001.

3. Results

3.1 Dataset characterization

The GSE14668 dataset had 8 liver specimens obtained from 2 HBV-associated ALF patients, 8 individual liver specimens from 8 liver donors and 11 normal liver specimens from 11 patients who underwent resection for angioma. GSE62029 had 13 liver specimens obtained from 4 HBV-associated ALF patients, 10 individual liver specimens from 10 liver donors and 7 normal liver specimens from 7 patients who underwent resection for angioma. GSE74000 had 3 specimens obtained from one acetaminophen (APAP)-induced ALF patient and 2 healthy livers from individuals deceased from brain damage. All three datasets are from the GPL570 platform (Table 1).

unedited

Table 1 Information of three datasets

Name	Etiology	Number				Platform
		ALF patient	ALF sample	Donor	Liver Angioma	
GSE14668	HBV	2	8	8	11	GPL570
GSE62029	HBV	4	13	10	7	GPL570
GSE74000	APAP	1	3	1(2)&	0	GPL570

&Note: GSE74000 contains one donor, but the donor contributes two samples

3.2 Identification of DEGs

The intersection of the three datasets is shown in Fig. 2A. Batch effects were removed to obtain the integrated dataset (Fig. 2B-E). A total of 5113 genes were identified as DEGs using the Limma method, of which 3136 were up-regulated and 1977 down-regulated. A heatmap and volcano plot of the ALF DGEs are shown in Fig. 2F, G.

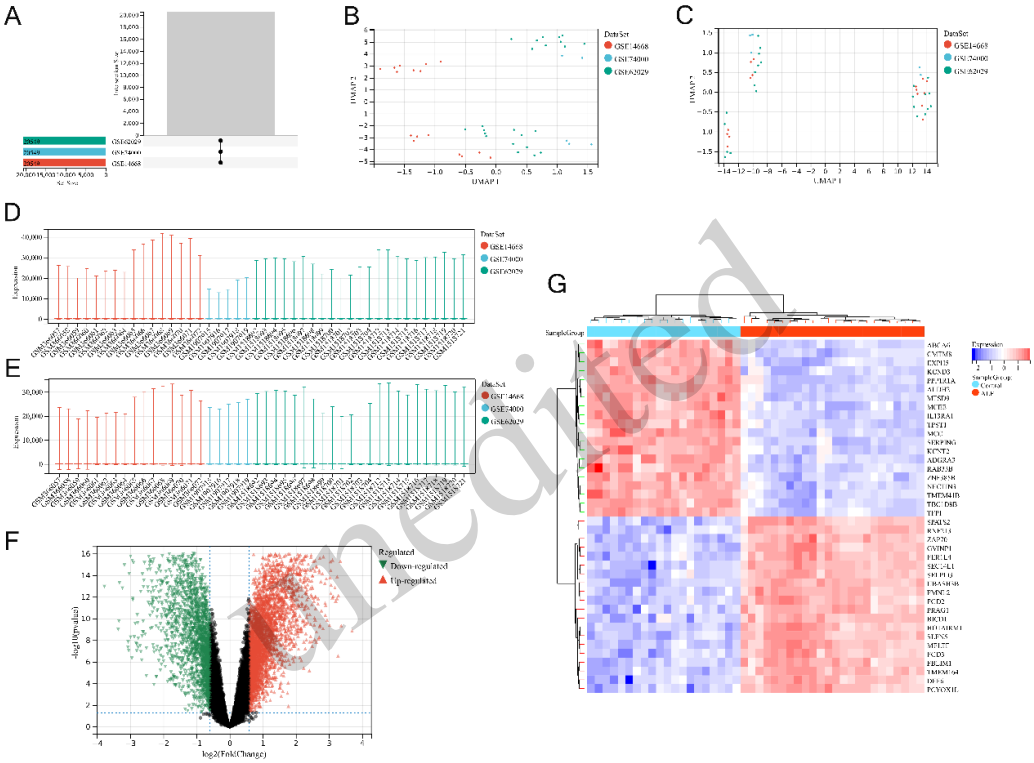

Fig. 2 Screening for differential genes. (A) Intersection size of the three datasets. (B, C) Gene expression level statistics of the datasets before and after de-batching. (D, E) Principal component analysis (PCA) among datasets before and after de-batching. (F) A volcano plot of DEGs: up-regulated DEGs are represented by red nodes, down-regulated DEGs by green nodes, and genes with no significant differential expression by black nodes. (G) Heat map of DEG expression levels: azure indicates control samples, orange indicates ALF samples, red indicates high gene expression and purple indicates low gene expression.

3.3 Weighted gene co-expression network analysis and key module identification

WCGNA was applied to explore the differences in gene expression between the ALF group and the control group. We chose β=24 as the "soft" threshold because it was the first power value when the index of scale-free topologies reached 0.85 (Fig. 3A, B). Nine gene co-expression modules (GCMs) discovered based on this power are shown in different colors (Fig. 3C, D). The correlation between ALF and GCMs is presented in Fig. 3E. The mediumpurple3 module (1484 genes) was identified as the pivotal module for subsequent analysis since it had the highest correlation with ALF (correlation coefficient =0.88, P=1.8*10^{-15}). Additionally, a significant positive correlation was observed between gene significance and module membership (r=0.8) (Fig. 3F). According to the above results, we believe that mediumpurple3 module genes were most

Unedited

significantly associated with ALF.

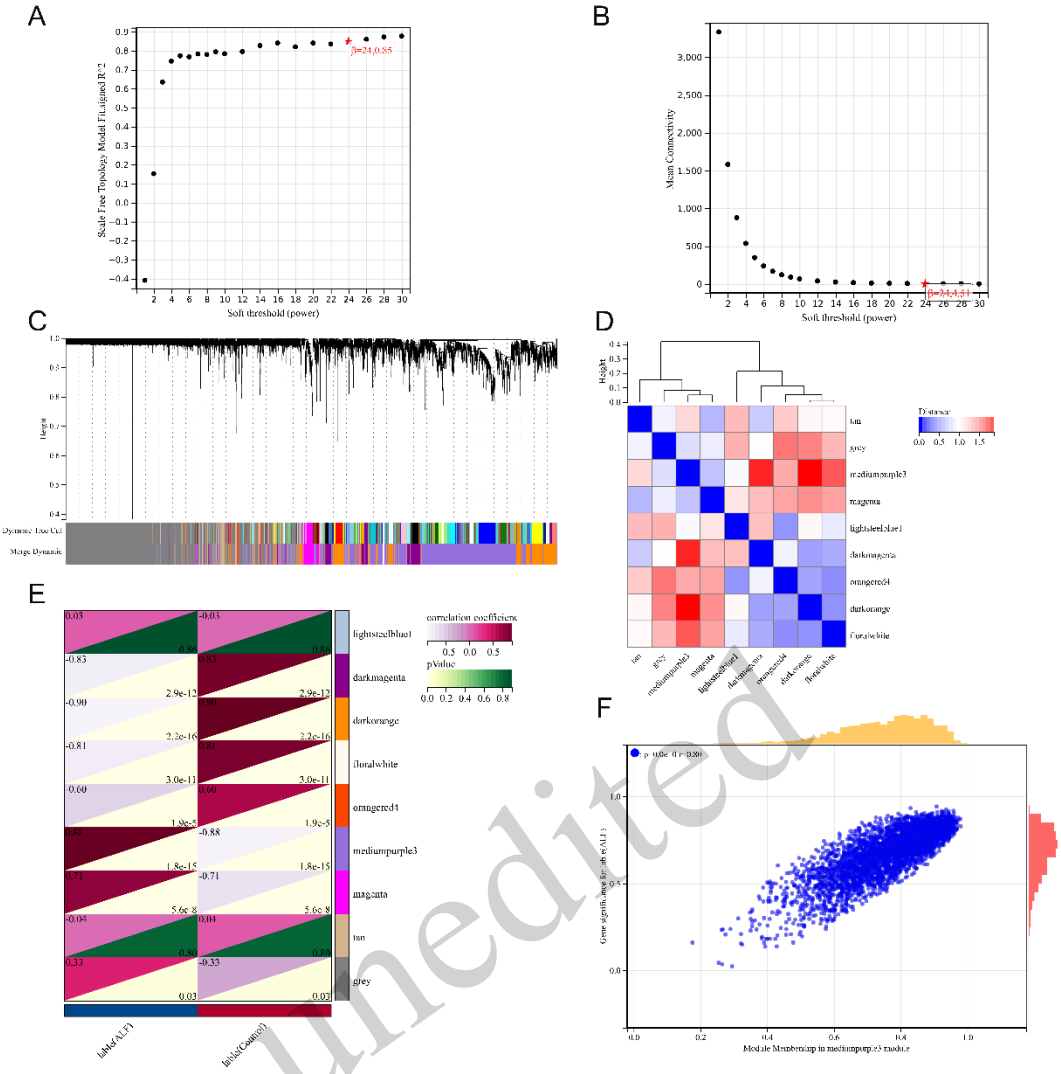

unedited

Fig. 3 Weighted gene co-expression network analysis. (A, B) Analysis of the scale-free fit index for various soft-thresholding powers. (C) Gene trees of co-expression gene modules are shown in various colors. (D) Heatmap of eigengene adjacency. (E) Heatmap of the association between ALF and modules. The mediumpurple3 module is shown to be correlated significantly with ALF. Numbers in the top and bottom triangles represent the correlation coefficient and p-value, respectively. (F) Correlation plot between gene significance and module membership of genes included in the mediumpurple3 module.

3.4 Screening and characterization of hub genes

Seven hub genes, namely BMF, BNIP3L, CASP1, RIPK3, UACA, UNC5B, and ZBP1, were obtained after intersecting 5113 DEGs, 1484 genes in the “mediumpurple3 module” of WCGNA and 75 genes related with PANoptosis, using the Venn diagram tool (Fig. 4A, Table 2). Fig. 4B shows the potential interaction between the 7 hub genes. UNC5B could link to the contacting network through NTN1 and CTSB and UACA through BCL2L1. In addition, CASP8 seems to have great importance in this network. Next, GO and KEGG enrichment analyses were performed to reveal the function of PANoptosis-related genes. The PANoptosis-related genes were enriched mainly in pathways involved in the defense response to viruses, positive regulation of hydrolase activity, cytosolic DNA-sensing pathway, regulation of mitochondrion organization, pyroptosis and positive regulation of the necroptotic process (Fig. 4C). Besides, all hub genes were up-regulated in the ALF group (Fig. 5A-G).

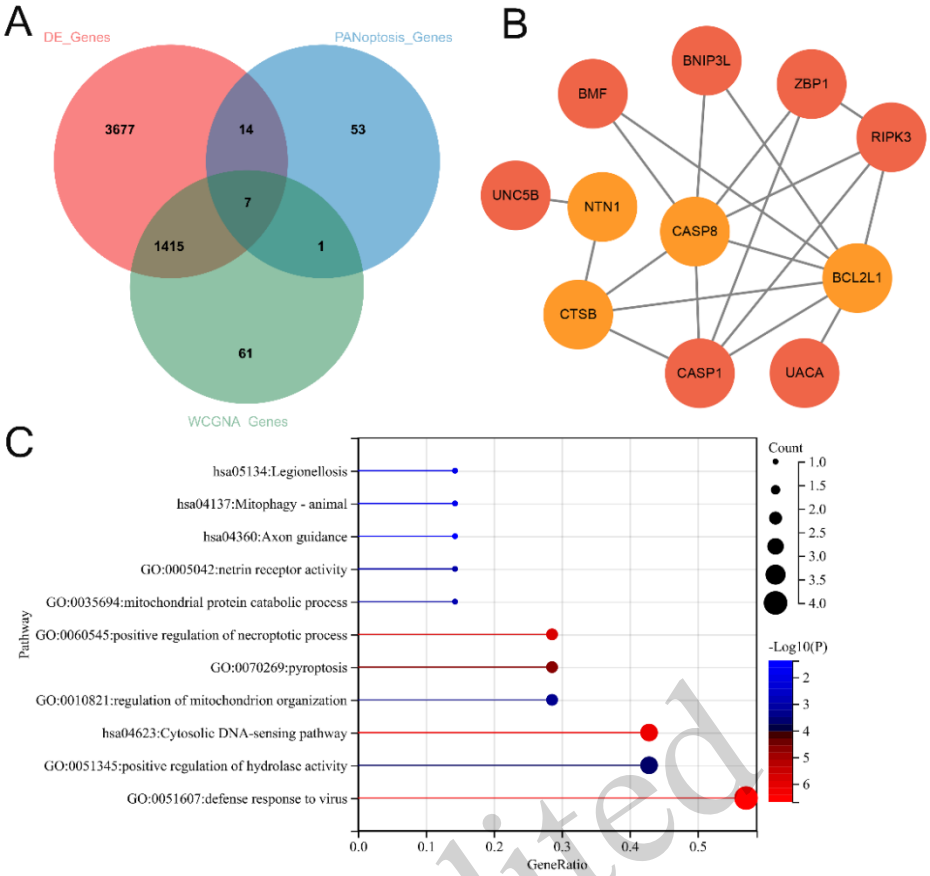

unedited

Fig. 4 Selection of the PANoptosis-related genes. (A) Venn diagram showing the seven PANoptosis-related genes from the intersection of DEGs, mediumpurple3 module via WCGNA and 75 genes that refer to PANoptosis. (B) PPI network revealed that the seven hub genes were linked directly or indirectly. The genes in the orange circle are the hub genes, and those in the yellow circle are the bridge genes needed to connect the hub genes (C) Enrichment analysis of KEGG and GO pathways related to the seven hub genes.

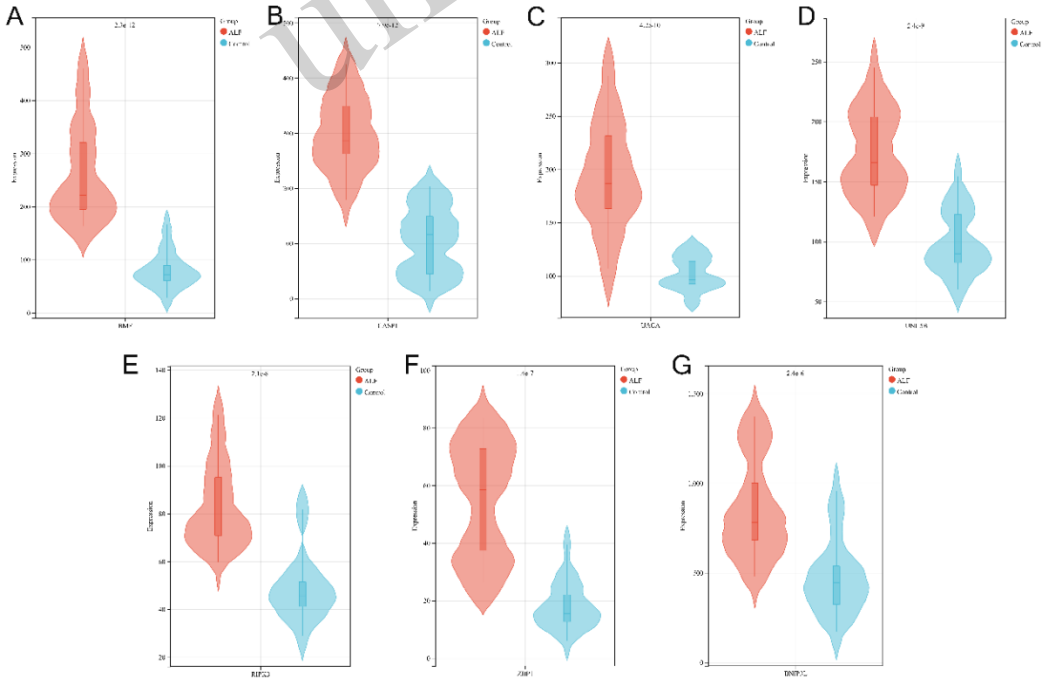

Fig. 5 Violin plots of the expression of seven PANoptosis-related genes in the ALF and control groups. (A) Expression of BMF. (B) Expression of CASP1. (C) Expression of UACA. (D) Expression of UNC5B. (E) Expression of RIPK3. (F) Expression of ZBP1. (G) Expression of BNIP3L. *P* <0.0001.

Table 2. Gene set related to PANoptosis

Gene name						
AIFM1	AKT3	APAF1	APPL1	BAK1	BAX	BMF
BNIP3L	BOK	CASP1	CASP10	CASP2	CASP3	CASP4
CASP5	CASP6	CASP7	CASP8	CD14	CHMP2A	CHMP2B
CHMP3	CHMP4A	CHMP4B	CHMP4C	CHMP6	CHMP7	CHUK
CRADD	CYCS	DFFA	DFFB	E2F1	ELANE	FADD
FADD	FAS	FASLG	GSDMD	GSDME	GZMB	HMGB1
HMGB2	IGF1	IL18	IL1A	IL1B	IRF1	IRF2
LY96	MAP3K7	MLKL	NLRP3	PPP3R1	PSTPIP2	PYCARD
RBCK1	RIPK1	RIPK3	RNF31	TFDP1	TICAM1	TLR3
TNF	TNFAIP3	TNFRSF1A	TNFSF10	TP63	TP73	TRAF2
UACA	UNC5B	YWHAE	YWHAG	ZBP1		

3.5 GSEA enrichment of seven PANoptosis-related genes

To further identify the associated signaling pathways of the seven PANoptosis-related genes, we used GSEA software to perform a single gene differential analysis between the ALF group and the control group. Seven PANoptosis-related genes were positively correlated with part of the signaling pathways CELL_ADHESION_MOLECULES_CAMS, CHEMOKINE_SINALING_PATHWAY, LYSOME. PRIMARY_IMMUNODEFICIENCY, and ANTIGEN_PROCESSING_AND_PRESENTATION, but negatively correlated with PEROXISOME, except BNIP3L (Fig. 6A-G).

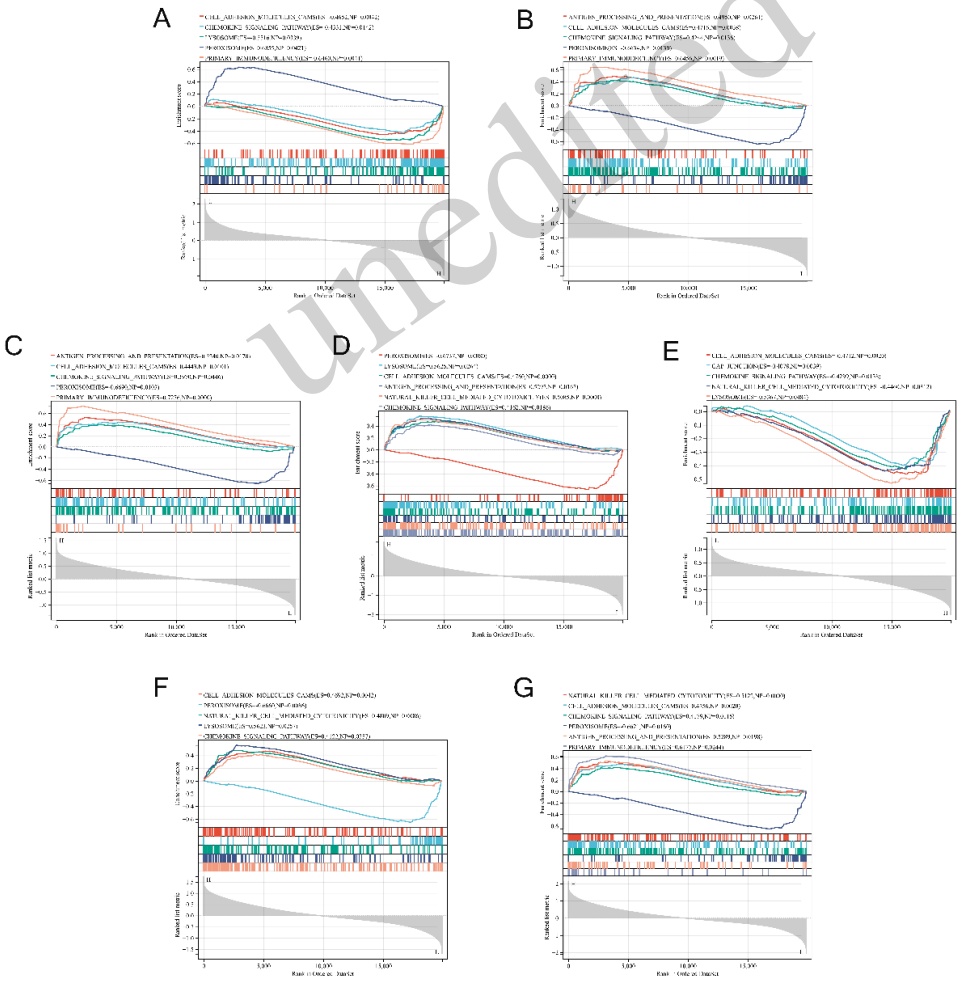

unedited

Fig. 6 GSEA of seven PANoptosis-related genes. (A) GSEA of CASP1. (B) GSEA of RIPK3. (C) GSEA of ZBP1. (D) GSEA of BMF. (E) GSEA of BNIP3L. (F) GSEA of UNC5B. (G) GSEA of UACA.

3.6 Immune cell infiltration in ALF

CIBERSORT is an appropriate algorithm for investigating the connections between characteristic genes and immune cells. We used CIBERSORT to examine the mechanisms that link feature genes to immune cell infiltration in ALF. The infiltration of immune cells in ALF is depicted in Fig. 7A. Compared with the control group, the ALF group exhibited a significantly higher abundance of memory B cells, CD8 T cells, naïve CD4 T cells , T cells, CD4 memory activated monocytes, and M2 macrophages (Fig. 7C). Furthermore, we explored the association between feature genes and immune cells. Except for BNIP3L, the other six PANoptosis-related genes were all negatively associated with activated dendritic cells, activated mast cells and neutrophils. BMF, CASP1, UACA and ZBP1 exhibited a positive correlation with naïve CD4 T cells and memory activated CD4 T cells, while BNIP3L showed a positive correlation with only naïve CD4 T cells. Also, BMF, CASP1 and ZBP1 were negatively correlated with some or all of these immune cells: macrophage infiltration, activated NK cells and follicular helper T cells (Fig. 7B). These findings indicate that the feature genes are closely linked to immune cell infiltration in the liver and play a critical role in shaping the immune microenvironment in ALF.

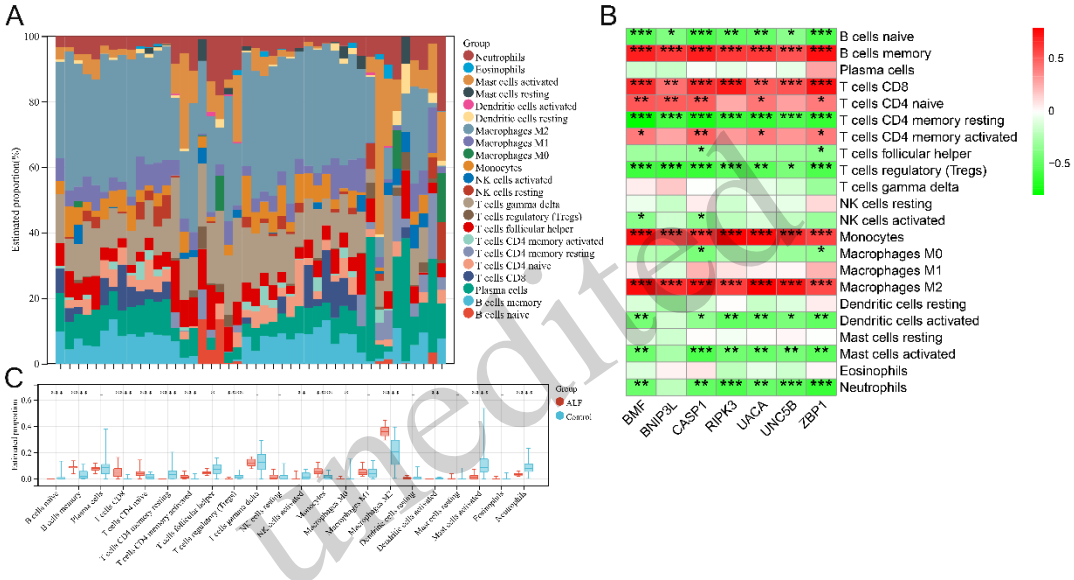

unedited

Fig. 7 Immune cell infiltration in ALF. (A) The proportion of 22 types of immune cells in ALF and control groups. (B) Correlations among seven PANoptosis-related genes and 22 immune cell types. (C) Comparison of the proportions of 22 kinds of immune cell between ALF and control groups. (*, *P* <0.05; **, *P* <0.01; *, *P* <0.001; ****, *P* <0.0001).**

3.7 Experimental verification of the ALF mouse model

First, we established an LPS-induced acute liver injury model and observed significant congestion in the livers of mice 6 h after LPS/D-gal injection (Fig. 8A). To investigate the dynamic changes in acute liver injury, we set up different modeling time points. We found that the serum levels of ALT and AST showed no significant changes in mice with early-stage liver failure, but suddenly increased at 6 h, exhibiting a sharp increase (Fig. 8B). Cytokines showed dynamic changes as well. TNF-α gradually increased after LPS injection, reaching its peak 1 h after modeling, followed by a gradual decrease. IFN-γ increased only at 4 h after injection, followed by a decrease, while IL-6 peaked 2 h after modeling and gradually declined. The anti-inflammatory factor IL-10 peaked at 1 h and then gradually decreased.

To explore the dynamic changes of PANoptosis-related genes in the mouse liver, we conducted western blot analysis on liver tissue homogenates at various time points. As shown in Fig. 8C, the expression of P-RIPK3, RIPK3, UACA, ZBP1, BNIP3L, and BMF began to increase after LPS injection, but their peak times and change trends were different. The peak expression time of RIPK3 was 0.5 h after modeling while for P-RIPK3 it was 1 h, indicating that RIPK3 and its

function were activated early on. The peak expression of UACA occurred 4 h after modeling and lasted longer. ZBP1 expression was observed mainly between 0.5 and 2 h. BNIP3L expression gradually increased, peaking at 6 h of modeling, possibly related to ALT and AST expression. The peak expression of BMF occurred at 4 h, but its change amplitude was not significant. UNC5B expression levels gradually decreased, suggesting it may be a protective protein. The expression of CASP1 also gradually decreased, but the amount of cleaved caspase1 increased during the modeling.

Next, we explored the cellular localization of the seven target genes. According to the WB results, all seven genes were expressed 4 h after modeling, so we selected the liver sections sampled at that time point. As shown in the Fig 8D, the expression of BMF and UNC5B was low in macrophages (golden arrow). BNIP3L and F4/80 expression overlapped almost completely, indicating that BNIP3L was expressed mainly in F4/80^{+}macrophages. There was good overlap between CASP1/RIPK3/UACA and CD11b, which confirmed that these three genes were expressed mainly in F4/80^{+}, CD11b^{+} and ly6c^{+} monocyte derived macrophages (MoMFs). ZBP1 overlapped well with DAPI, indicating that ZBP1 is expressed mainly in the nucleus. The immunofluorescence results showed that macrophages expressed these seven genes, but the genes were not expressed only on macrophages.

unedited

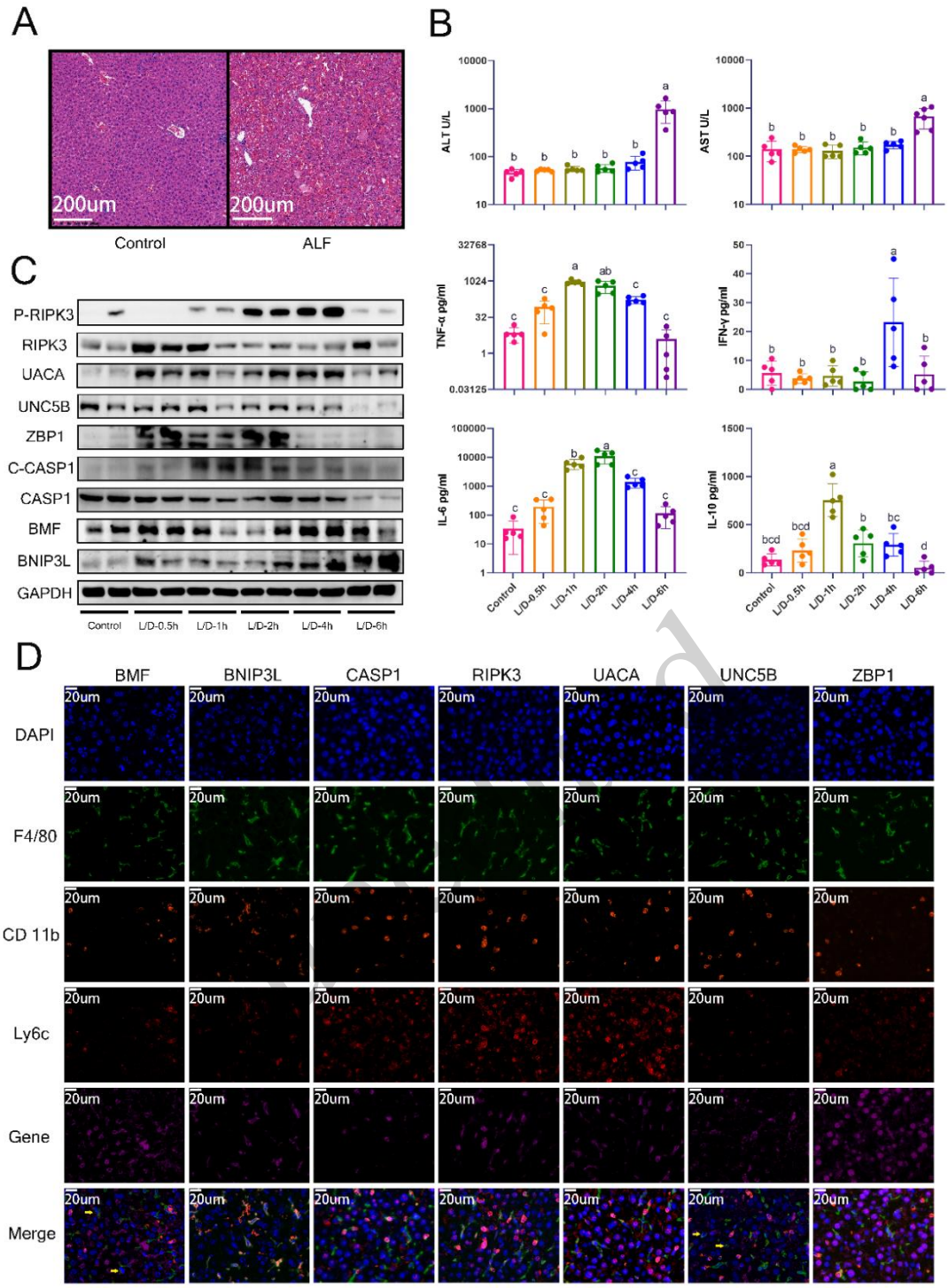

Fig. 8 Verification of the animal model. (A) Hematoxylin and eosin (H&E) staining of liver sections. (B) Levels of serum ALT, AST, TNF-α, IFN-γ, IL-6, and IL-10. (C) Changes of the expression levels of 9 kinds of proteins with the time of modeling, by western blot. (D) Cellular localization analysis of the seven genes through immunofluorescence with TSA. C-CASP1 denotes cleaved caspase1. The presence of the same letter between two groups indicates no significant difference between them, and the absence of the same letter indicates a significant statistical difference between them (*P* <0.05).

Immune cells in the liver are mainly macrophages, and the results of immune infiltration showed that all seven molecules were closely associated with monocytes and macrophages. Therefore, we performed flow cytometric analysis on liver macrophages. We observed that

Kupffer cells showed a trend of an initial decrease followed by reduction, while peripheral monocytes showed a trend of initial increase followed by reduction, with both reaching their peak values at 1 h, indicating a complementary pattern (Fig. 9A,B) (P <0.05).

To further confirm the reliability of the flow results, the liver sections were stained by immunofluorescence. We found that the number of macrophages of F4/80$^+$ and CD11b$^+$ decreased immediately within 0.5 h after LPS/D-gal stimulation, and then increased, reaching a peak at 6 h after LPS/D-gal stimulation. Ly6c$^+$ macrophages also decreased within 0.5 h after LPS/D-gal stimulation, then increased slowly, reaching a peak at 4 h, and then decreased at 6 h (Fig. 9C). Although the time point of the minimum value differs from that of the flow diagram, the general trend is consistent with the change shown by the flow results. In addition, we also measured the average fluorescence intensity (AVI) of ly6c$^+$ cells and found that it decreased after LPS/D-gal stimulation, then gradually increased, reaching a peak at 4 h, and then declined. Since MoMFs are cells highly expressing ly6c (Fig.9D), this may indicate that the increased macrophages in the liver after LPS/D-gal stimulation are derived from peripheral monocytes.

As PANoptosis has the characteristics of pyroptosis, apoptosis and necroptosis, we detected the markers of these three modes of cell death. The expression of MLKL decreased at 6 h after modeling, while the expression of its activation product P-MLKL was high before 2 h and then gradually decreased, indicating that necroptosis occurs mainly in the early stage of ALF. This result was basically consistent with p-ripk3. GSDME expression increased significantly at 6 h after modeling, and cleaved GSDMD expression decreased immediately after stimulation with LPS/D-gal, indicating that the factor inducing pyroptosis gradually changed from GSDMD to GSDME with disease progression. Apoptotic markers, cleaved caspase3 and cleaved caspase8, were significantly increased at the end stage of liver failure, indicating that apoptosis was also present at the stage of liver failure (Fig. 9E). Both pyroptosis and apoptosis occur in the end stage of ALF, and all three cell death modes occur in the development of ALF. This shows that the cell death modes are not independent of each other, and further highlights the importance of PANoptosis in ALF.

Finally, PANoptosis is a process of cell death mediated by PANoptosomes. The detection of PANoptosomes is the gold standard for confirming the occurrence of PANoptosis. For this purpose, we isolated BMDMs from mice and constructed a cell model of ALF with LPS stimulation. Subsequently, PANoptosomes were detected by immunofluorescence combined with the TSA technique. We found that compared with the control group, PANoptosomes composed of ZBP1, RIPK3, CASP1, and CASP8 were formed in BMDM cells after LPS stimulation, as shown by the obvious overlapping of immunofluorescence of the four proteins observed under the microscope (Fig. 9F, yellow arrows). This indicates that BMDMs undergo PANoptosis after LPS stimulation. MoMFs are similar to BMDMs in that they are also derived from bone marrow monocytes. Therefore, we believe that the PANoptosis of macrophages promotes the occurrence and development of ALF (Fig. 9F).

unedited

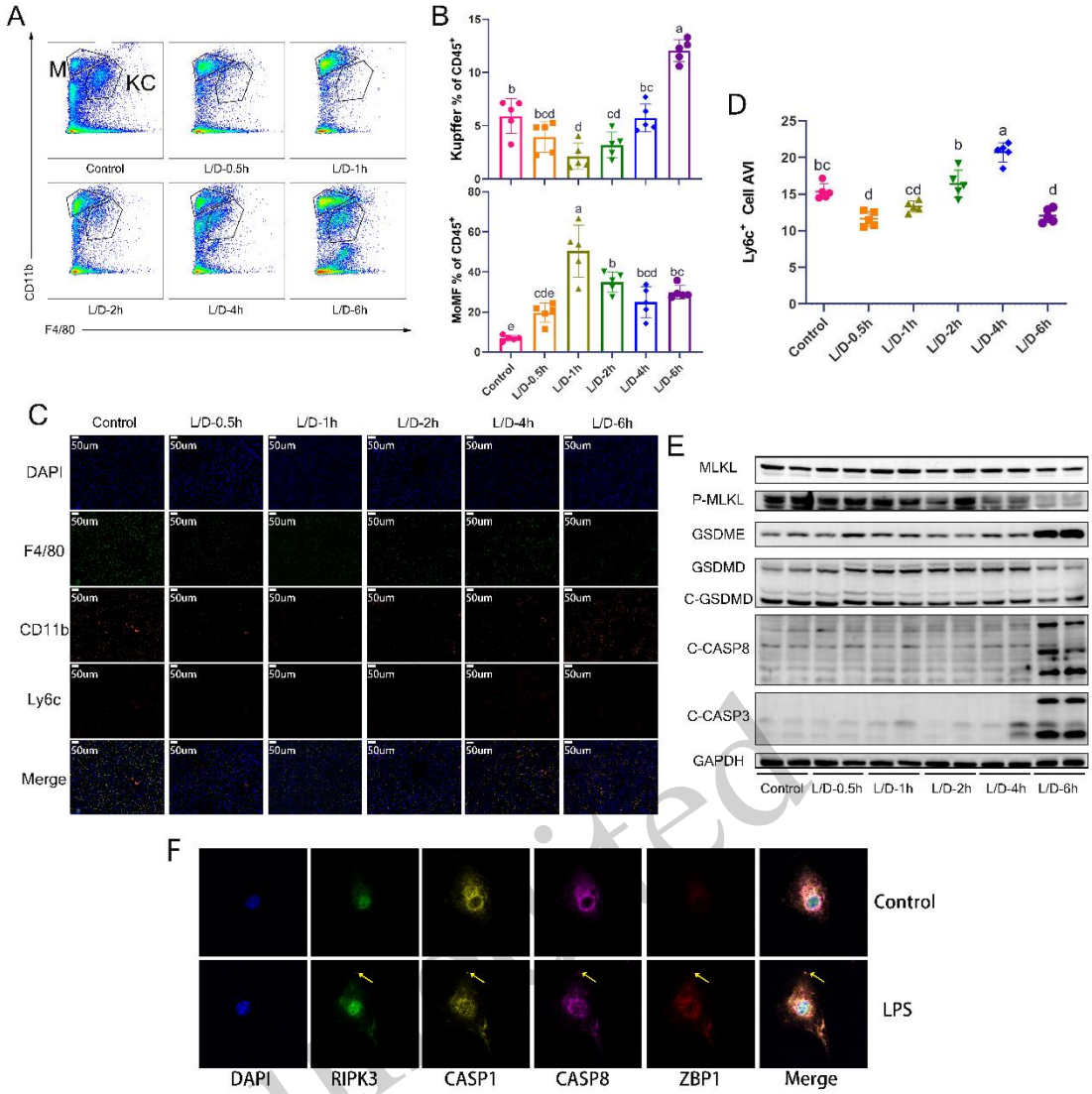

Fig. 9 The change trend of macrophages, pyroptosis, apoptosis and necroptosis in the liver after LPS/D-gal stimulation. (A) Representative flow cytometry plots of Kupffer cells (labeled KC) and MoMFs (labeled M) of each group. (B) Percentage of Kupffer cells and MoMFs in hepatic CD45$^+$ cells. (C) Immunofluorescence results of macrophages in liver tissue at different time points after LPS/D-gal stimulation. (D) Average fluorescence intensity (AVI) of ly6c+ cells. (E) Trends of biomarkers of pyroptosis, apoptosis and necroptosis. (F) Immunofluorescence results of PANoptosomes in BMDMs after LPS stimulation for 6 h (63x oil). The presence of the same letter between two groups indicates no significant difference between them, and the absence of the same letter indicates a significant statistical difference between them (*P* <0.05). C-GSDMD means cleaved GSDMD, C-CASP8 means cleaved caspase8, and C-CASP3 means cleaved caspase3.

4. Discussion

In recent years, the combination of microarray and sequencing methods with integrative bioinformatics analysis has been used increasingly to investigate potential diagnostic biomarkers, underlying mechanisms, and prospective therapeutic targets of diseases (Petrik, 2006; Su et al., 2011).

Although there are numerous factors that can lead to ALF, the central common factor is the cytokine storm triggered by an immune response. Previously, the main focus was on studying the cytokine storm associated with specific types of cell death, such as pyroptosis, apoptosis, and necroptosis, overlooking the interconnections among the different forms of cell death (Duan et al., 2022; Huo et al., 2023; Li et al., 2023; Vasudevan et al., 2023). Hence, the identification of

PANoptosis effectively addresses this gap. Presently, studies on PANoptosis concentrate mainly on cancer and COVID-19 (Karki et al., 2021a; Karki, et al., 2021b). As far as we know, this research represents the first exploration of the potential link between ALF and PANoptosis, potentially unveiling new targets for the future prevention, diagnosis, and treatment of ALF.

Despite the complex and diverse etiology of ALF, including factors such as infections, drug toxicity, and autoimmune reactions, immune reactions play a role in nearly all instances of the disease (Bernal and Wendon, 2013; Stravitz and Lee, 2019), with similarities observed in these immune reactions across different scenarios. Based on this foundation, in this study we integrated three ALF databases with distinct etiologies to yield more comprehensive findings. Initially, 5113 DEGs were identified from the combined dataset. Subsequently, we used the WGCNA method to categorize these genes functionally and identify gene modules with notable differences. Ultimately, we intersected these results with a gene set related to PANoptosis to identify seven key target genes. While obtaining the PANoptosis-related gene set, consensus had not been reached on genes associated with PANoptosis. Therefore, we assembled a PANoptosis-related gene set comprising 75 genes by merging genes involved in processes like pyroptosis, apoptosis, and necroptosis, along with genes shown to be involved in PANoptosis (Pan et al., 2022). The progression of ALF relies on the interactions of genes. As indicated by the violin plot, the expression of the 7 feature genes was consistently higher in the ALF group than in the control group, underscoring their pivotal role in the pathophysiology of ALF.

Early biochemical analyses showed that BMF was associated with actin filaments in the cytoskeleton. Under certain cellular stress conditions, BMF can change subcellular localization, and then transfer into mitochondria and co-immunoprecipitate with bcl2 to trigger apoptosis, which may be mediated by the TGF-β signaling pathway through the activation of Runx3 (Puthalakath et al., 2001; Puthalakath and Strasser, 2002; Yamamura et al., 2006; Ramjaun et al., 2007). Early studies indicated that a hypoxic environment stimulates the up-regulation of BNIP3Lvia HIF-1, and subsequent research has confirmed that BNIP3L can trigger mitophagy (Sowter et al., 2001; Chen et al., 2023; Verbeke et al., 2023). In advanced stages of ALF, impaired coagulation function can lead to tissue hypoxia, resulting in increased expression of BNIP3L. Furthermore, western blot analysis of mouse tissues shows that after 6 h of modeling, severe liver congestion is evident, with peak BNIP3L expression observed at this stage. Perhaps inhibiting BNIP3L could alleviate the progression of ALF, or BNIP3L could serve as a predictive molecule. Currently, research on CASP1 focuses mainly on two aspects: the CASP1-dependent canonical pyroptosis pathway, and the NLRP3/CASP1 inflammasome pathway (Wang et al., 2017; Yu et al., 2023). Our western blot results in this study indicate a decrease in CASP1 expression levels in the late stages of modeling, while the expression level of the activated type of cleaved caspase1 increased. These changes are possibly attributed to the pronounced liver congestion and hypoxic conditions prevalent in the tissue at this stage of modeling. This observation is consistent with past studies indicating that HIF-1 can activate the NLRP3/CASP1 signaling pathway (Jiang et al., 2022). In vitro experiments also showed a correlation between hypoxia and the NLRP3/ASC/CASP1 signaling axis (Slowik et al., 2018). RIPK1/RIPK3/MLKL constitutes the core of the necroptosis signaling pathway. Upon activation of TLR4 by LPS, RIPK1 is indirectly recruited through TRIF (TIR-domain-containing adapter-inducing interferon β). Accompanied by the inhibition of CASPASE8 activity, RIPK3 is activated and recruits MLKL later. Phosphorylation of MLKL by RIPK3 leads to its translocation to the cell membrane, ultimately resulting in cell rupture (Newton, 2015). Research indicates that RIPK1 and RIPK3 can activate the NLRP3 inflammasome and contribute to autoimmune diseases (Speir and Lawlor, 2021). Our western blot results showed that RIPK3 is activated within just 0.5 h after modeling, suggesting that necroptosis is the earliest form of cell death. Monitoring markers associated with necroptosis could potentially act as a valuable early detection tool. UACA could interact with Apaf-1 and translocate it into the nucleus under proapoptotic stress to induce apoptosis (Sakai et al., 2003; Ohkura et al., 2004). Also, UACA interacted with the nuclear factor-κB (NF-κB) to reduce the expression of the NF-κB targeted genes (Liu et al., 2009). In this study, the expression level of

unedited

UACA consistently increased during the modeling process and decreased towards the later stages. We believe that the initial increase in expression is aimed mainly at inducing apoptosis, while the subsequent decrease in expression is intended to enhance the expression of NF-κB target genes. The UNC5B signaling pathway involves monocyte differentiation into macrophages, macrophage infiltration, angiogenesis, cell apoptosis, and endoplasmic reticulum stress (Koch et al., 2011; Choi et al., 2022; Huang et al., 2022; Fang et al., 2023; Yang et al., 2023). Research suggests that the absence of UNC5B exacerbates tissue injury in acute kidney injury. In our research, we observed a decrease in Unc5b expression as the modeling time prolonged, confirming its protective function. This trend was also supported by the flow cytometry results. The initial increase followed by a decrease in peripheral monocytes is attributed to the reduction in UNC5B expression in the early stages of modeling being insufficient to prevent the recruitment and differentiation of peripheral monocytes, whereas the subsequent decrease is due to insufficient UNC5B. The later decrease in peripheral monocytes is due to insufficient Unc5b levels. Similarly, the initial decrease and subsequent increase in KCs are a result of MoMFs acquiring a KC-like phenotype after acute or specific KC depletion under various signaling influences (Adrien and Frank, 2023). ZBP1 is a crucial initiator of both innate immune responses and PANoptosis. Its activation of innate immune responses includes type I interferon response and NF-κB signaling, forming a critical defense line against pathogenic infections. ZBP1-mediated PANoptosis presents a double-edged sword: it can eliminate infected cells and tumor cells, but excessive PANoptosis can trigger a cytokine storm and pose harm to the host. Our WB results also showed that ZBP1 expression increased in the initial phases of modeling, further confirming its role as an initiator (Takaoka et al., 2007; Rebsamen et al., 2009; Hao et al., 2022). Subsequently, we conducted an analysis of the cellular localization of seven genes via immunofluorescence. Results showed that macrophages can express these seven genes. Next, we investigated the markers of pyroptosis, apoptosis, and necroptosis, revealing that the three types of RCD are intertwined throughout the progression of ALF, which further emphasizes the importance of PANoptosis in ALF. Finally, using the cell model of ALF, we confirmed that macrophages could form PANoptosomes to induce PANoptosis.

This study, encompassing database analysis and animal studies, highlights the pivotal role of PANoptosis in the onset and progression of ALF. However, it had several limitations. Firstly, the data were obtained from public databases, which imposed limitations on sample size. Secondly, the lack of consensus on PANoptosis-related genes may result in certain omissions. Thirdly, although we validated the expression of relevant genes in the mouse liver, their underlying mechanisms have not been further verified. Lastly, the challenge of acquiring clinical ALF samples prevented us from obtaining further validation from patients. Nevertheless, our study has provided valuable and novel insights.

unedited

5. Conclusions

Our study revealed new insights into the development and progression of ALF by using advanced bioinformatics techniques. We successfully identified and confirmed the roles of 7 PANoptosis-related genes, and validated the involvement of macrophages in this process. This discovery has the potential to significantly impact the development of diagnostic markers and treatment strategies for ALF, as we gain a deeper understanding of its molecular mechanisms.

Data availability statement

The dataset used or analyzed during the current study is available from the corresponding author on reasonable request.

Acknowledgments

This work was supported by the National Science and Technology Major Project of China (2018ZX10302206).

Author Contributions

Zhi Chen and Junwei Shao contributed to the study conception and design; Tiantian Ge and Yao Chen contributed to data collection, assembly, analysis and interpretation of the data; Tiantian Ge and Lantian Pang contributed to the animal experiment; Tiantian Ge and Yao Chen contributed to the manuscript drafting; Zhi Chen and Junwei Shao contributed to the revising and approval of the final version of the manuscript. All authors have read and approved the final manuscript.

Compliance with ethics guidelines

Tiantian Ge, Yao Chen, Lantian Pang, Junwei Shao and Zhi Chen declare that they have no conflict of interest.

The animal experiments adhered to the ethical principles outlined in the Declaration of Helsinki and received approval from the research ethics committee of the First Affiliated Hospital of Zhejiang University School of Medicine (20211404).

References

Adrien G, Frank T, 2023. Spatial dimension of macrophage heterogeneity in liver diseases. *eGastroenterology*, 1(1):e000003. https://doi.org/10.1136/egastro-2023-000003

Bernal W, Wendon J, 2013. Acute liver failure. *N Engl J Med*, 369(26):2525-2534. https://doi.org/10.1056/NEJMra1208937

Chen Y, Jiao D, Liu Y, et al., 2023. Fbxl4 mutations cause excessive mitophagy via bnip3/bnip3l accumulation leading to mitochondrial DNA depletion syndrome. *Cell Death Differ*, https://doi.org/10.1038/s41418-023-01205-1

Choi SW, Oh H, Park SY, et al., 2022. Netrin-1 attenuates hepatic steatosis via unc5b/ppargamma-mediated suppression of inflammation and er stress. *Life Sci*, 311(Pt B):121149. https://doi.org/10.1016/j.lfs.2022.121149

Christgen S, Zheng M, Kesavardhana S, et al., 2020. Identification of the panoptosome: A molecular platform triggering pyroptosis, apoptosis, and necroptosis (panoptosis). *Front Cell Infect Microbiol*, 10:237. https://doi.org/10.3389/fcimb.2020.00237

Duan YW, Chen SX, Li QY, et al., 2022. Neuroimmune mechanisms underlying neuropathic pain: The potential role of tnf-alpha-necroptosis pathway. *Int J Mol Sci*, 23(13) https://doi.org/10.3390/ijms23137191

Fang Y, Ma K, Huang YM, et al., 2023. Fibronectin leucine-rich transmembrane protein 2 drives monocyte differentiation into macrophages via the unc5b-akt/mtor axis. *Front Immunol*, 14:1162004. https://doi.org/10.3389/fimmu.2023.1162004

Galluzzi L, Kepp O, Krautwald S, et al., 2014. Molecular mechanisms of regulated necrosis. *Semin Cell Dev Biol*, 35:24-32. https://doi.org/10.1016/j.semcdb.2014.02.006

Galluzzi L, Bravo-San Pedro JM, Vitale I, et al., 2015. Essential versus accessory aspects of cell death: Recommendations of the nccd 2015. *Cell Death Differ*, 22(1):58-73. https://doi.org/10.1038/cdd.2014.137

Green DR, Kroemer G, 2005. Pharmacological manipulation of cell death: Clinical applications in sight? *J Clin Invest*, 115(10):2610-2617. https://doi.org/10.1172/JCI26321

Hao Y, Yang B, Yang J, et al., 2022. Zbp1: A powerful innate immune sensor and double-edged sword in host immunity. *Int J Mol Sci*, 23(18) https://doi.org/10.3390/ijms231810224

Huang L, An X, Zhu Y, et al., 2022. Netrin-1 induces the anti-apoptotic and pro-survival effects of b-all cells through the unc5b-mapk axis. *Cell Commun Signal*, 20(1):122. https://doi.org/10.1186/s12964-022-00935-y

Huo C, Tang Y, Li X, et al., 2023. Melatonin alleviates lung injury in h1n1-infected mice by mast cell inactivation and cytokine storm suppression. *PLoS Pathog*, 19(5):e1011406. https://doi.org/10.1371/journal.ppat.1011406

Jiang W, Sun S, Wang D, et al., 2022. Microrna-22 suppresses nlrp3/casp1 inflammasome pathway-mediated proinflammatory cytokine production by targeting the hif-1alpha and nlrp3 in human dental pulp fibroblasts. *Int Endod J*, 55(11):1225-1240. https://doi.org/10.1111/iej.13814

Karki R, Sharma BR, Tuladhar S, et al., 2021a. Synergism of tnf-alpha and ifn-gamma triggers inflammatory cell death, tissue damage, and mortality in sars-cov-2 infection and cytokine shock syndromes. *Cell*, 184(1):149-168 e117. https://doi.org/10.1016/j.cell.2020.11.025

Karki R, Sundaram B, Sharma BR, et al., 2021b. Adar1 restricts zbp1-mediated immune response and panoptosis to promote tumorigenesis. *Cell Rep*, 37(3):109858. https://doi.org/10.1016/j.celrep.2021.109858

Khan SA, Shah N, Williams R, et al., 2006. Acute liver failure: A review. *Clin Liver Dis*, 10(2):239-258, vii-viii. https://doi.org/10.1016/j.cld.2006.05.010

Koch AW, Mathivet T, Larrivee B, et al., 2011. Robo4 maintains vessel integrity and inhibits angiogenesis by interacting with unc5b. *Dev Cell*, 20(1):33-46. https://doi.org/10.1016/j.devcel.2010.12.001

Kuriakose T, Man SM, Malireddi RK, et al., 2016. Zbp1/dai is an innate sensor of influenza virus triggering the

unedited

nlrp3 inflammasome and programmed cell death pathways. *Sci Immunol*, 1(2) https://doi.org/10.1126/sciimmunol.aag2045

Leek JT, Johnson WE, Parker HS, et al., 2012. The sva package for removing batch effects and other unwanted variation in high-throughput experiments. *Bioinformatics*, 28(6):882-883. https://doi.org/10.1093/bioinformatics/bts034

Li A, Yang Q, Lou G, et al., 2021. 5-((7-chloro-6-fluoro-1h-indol-3-yl) methyl)-3-methylimidazolidine-2,4-dione as a rip1 inhibitor protects lps/d-galactosamine-induced liver failure. *Life Sci*, 273:119304. https://doi.org/10.1016/j.lfs.2021.119304

Li X, Li X, Yang J, et al., 2023. In situ sustained macrophage-targeted nanomicelle-hydrogel microspheres for inhibiting osteoarthritis. *Research (Wash D C)*, 6:0131. https://doi.org/10.34133/research.0131

Lin JF, Hu PS, Wang YY, et al., 2022. Phosphorylated nfs1 weakens oxaliplatin-based chemosensitivity of colorectal cancer by preventing panoptosis. *Signal Transduct Target Ther*, 7(1):54. https://doi.org/10.1038/s41392-022-00889-0

Liu L, Sakai T, Tran NH, et al., 2009. Nucling interacts with nuclear factor-kappab, regulating its cellular distribution. *FEBS J*, 276(5):1459-1470. https://doi.org/10.1111/j.1742-4658.2009.06888.x

Long JS, Ryan KM, 2012. New frontiers in promoting tumour cell death: Targeting apoptosis, necroptosis and autophagy. *Oncogene*, 31(49):5045-5060. https://doi.org/10.1038/onc.2012.7

Malireddi RKS, Gurung P, Mavuluri J, et al., 2018. Tak1 restricts spontaneous nlrp3 activation and cell death to control myeloid proliferation. *J Exp Med*, 215(4):1023-1034. https://doi.org/10.1084/jem.20171922

Malireddi RKS, Kesavardhana S, Kanneganti TD, 2019. Zbp1 and tak1: Master regulators of nlrp3 inflammasome/pyroptosis, apoptosis, and necroptosis (pan-optosis). *Front Cell Infect Microbiol*, 9:406. https://doi.org/10.3389/fcimb.2019.00406

Newton K, 2015. Ripk1 and ripk3: Critical regulators of inflammation and cell death. *Trends Cell Biol*, 25(6):347-353. https://doi.org/10.1016/j.tcb.2015.01.001

Nguyen LN, Kanneganti TD, 2022. Panoptosis in viral infection: The missing puzzle piece in the cell death field. *J Mol Biol*, 434(4):167249. https://doi.org/10.1016/j.jmb.2021.167249

Ohkura T, Taniguchi S, Yamada K, et al., 2004. Detection of the novel autoantibody (anti-uaca antibody) in patients with graves' disease. *Biochem Biophys Res Commun*, 321(2):432-440. https://doi.org/10.1016/j.bbrc.2004.06.162

Pan H, Pan J, Li P, et al., 2022. Characterization of panoptosis patterns predicts survival and immunotherapy response in gastric cancer. *Clin Immunol*, 238:109019. https://doi.org/10.1016/j.clim.2022.109019

Petrik J, 2006. Diagnostic applications of microarrays. *Transfus Med*, 16(4):233-247. https://doi.org/10.1111/j.1365-3148.2006.00673.x

Puthalakath H, Villunger A, O'reilly LA, et al., 2001. Bmf: A proapoptotic bh3-only protein regulated by interaction with the myosin v actin motor complex, activated by anoikis. *Science*, 293(5536):1829-1832. https://doi.org/10.1126/science.1062257

Puthalakath H, Strasser A, 2002. Keeping killers on a tight leash: Transcriptional and post-translational control of the pro-apoptotic activity of bh3-only proteins. *Cell Death Differ*, 9(5):505-512. https://doi.org/10.1038/sj.cdd.4400998

Ramjaun AR, Tomlinson S, Eddaoudi A, et al., 2007. Upregulation of two bh3-only proteins, bmf and bim, during tgf beta-induced apoptosis. *Oncogene*, 26(7):970-981. https://doi.org/10.1038/sj.onc.1209852

Rebsamen M, Heinz LX, Meylan E, et al., 2009. Dai/zbp1 recruits rip1 and rip3 through rip homotypic interaction motifs to activate nf-kappab. *EMBO Rep*, 10(8):916-922. https://doi.org/10.1038/embor.2009.109

Sakai T, Liu L, Shishido Y, et al., 2003. Identification of a novel, embryonal carcinoma cell-associated molecule, nucling, that is up-regulated during cardiac muscle differentiation. *J Biochem*, 133(4):429-436. https://doi.org/10.1093/jb/mvg056

Schwabe RF, Luedde T, 2018. Apoptosis and necroptosis in the liver: A matter of life and death. *Nat Rev Gastroenterol Hepatol*, 15(12):738-752. https://doi.org/10.1038/s41575-018-0065-y

Slowik A, Lammerding L, Zendedel A, et al., 2018. Impact of steroid hormones e2 and p on the nlrp3/asc/casp1 axis in primary mouse astroglia and bv-2 cells after in vitro hypoxia. *J Steroid Biochem Mol Biol*, 183:18-26. https://doi.org/10.1016/j.jsbmb.2018.05.003

Sowter HM, Ratcliffe PJ, Watson P, et al., 2001. Hif-1-dependent regulation of hypoxic induction of the cell death factors bnip3 and nix in human tumors. *Cancer Res*, 61(18):6669-6673.

Speir M, Lawlor KE, 2021. Rip-roaring inflammation: Ripk1 and ripk3 driven nlrp3 inflammasome activation and autoinflammatory disease. *Semin Cell Dev Biol*, 109:114-124. https://doi.org/10.1016/j.semcdb.2020.07.011

Stravitz RT, Lee WM, 2019. Acute liver failure. *Lancet*, 394(10201):869-881. https://doi.org/10.1016/S0140-6736(19)31894-X

Su Z, Ning B, Fang H, et al., 2011. Next-generation sequencing and its applications in molecular diagnostics. *Expert Rev Mol Diagn*, 11(3):333-343. https://doi.org/10.1586/erm.11.3

Takaoka A, Wang Z, Choi MK, et al., 2007. Dai (dlm-1/zbp1) is a cytosolic DNA sensor and an activator of innate

Unedited

immune response. *Nature*, 448(7152):501-505. https://doi.org/10.1038/nature06013

Vasudevan SO, Behl B, Rathinam VA, 2023. Pyroptosis-induced inflammation and tissue damage. *Semin Immunol*, 69:101781. https://doi.org/10.1016/j.smim.2023.101781

Verbeke J, De Bolle X, Arnould T, 2023. When mitophagy dictates the outcome of cellular infection: The case of brucella abortus. *Autophagy*, :1-2. https://doi.org/10.1080/15548627.2023.2246354

Wang D, Zhang J, Jiang W, et al., 2017. The role of nlrp3-casp1 in inflammasome-mediated neuroinflammation and autophagy dysfunction in manganese-induced, hippocampal-dependent impairment of learning and memory ability. *Autophagy*, 13(5):914-927. https://doi.org/10.1080/15548627.2017.1293766

Wang Y, Chen Q, Jiao F, et al., 2021. Histone deacetylase 2 regulates ulk1 mediated pyroptosis during acute liver failure by the k68 acetylation site. *Cell Death Dis*, 12(1):55. https://doi.org/10.1038/s41419-020-03317-9

Yamamura Y, Lee WL, Inoue K, et al., 2006. Runx3 cooperates with foxo3a to induce apoptosis in gastric cancer cells. *J Biol Chem*, 281(8):5267-5276. https://doi.org/10.1074/jbc.M512151200

Yan WT, Zhao WJ, Hu XM, et al., 2023. Panoptosis-like cell death in ischemia/reperfusion injury of retinal neurons. *Neural Regen Res*, 18(2):357-363. https://doi.org/10.4103/1673-5374.346545

Yang X, Ma L, Zhang J, et al., 2023. Hypofucosylation of unc5b regulated by fut8 enhances macrophage emigration and prevents atherosclerosis. *Cell Biosci*, 13(1):13. https://doi.org/10.1186/s13578-023-00959-y

Yu X, Liu X, Liu X, et al., 2023. Overexpression of casp1 triggers acute promyelocytic leukemia cell pyroptosis and differentiation. *Eur J Pharmacol*, 945:175614. https://doi.org/10.1016/j.ejphar.2023.175614

Zheng Y, Sun W, Shan C, et al., 2022. Beta-hydroxybutyrate inhibits ferroptosis-mediated pancreatic damage in acute liver failure through the increase of h3k9bhb. *Cell Rep*, 41(12):111847. https://doi.org/10.1016/j.celrep.2022.111847

unedited